Synthesis, Structure, and Bonding of Butterfly Clusters Containing μ_4-Oxo and μ_4-Sulfido Ligands: [(PPh₃)₂N][Fe₃M(CO)₁₂(μ_4-E)] (E = O, S; M = Mn, Re)

Cynthia K. Schauer,[*,1a,b] Suzanne Harris,[*,1c] Michal Sabat,[1a,d] Eric J. Voss,[1a,e] and Duward F. Shriver[*,1a]

Department of Chemistry, Northwestern University, Evanston, Illinois 60208-3113, and Corporate Research Laboratory, Exxon Research and Engineering Company, Annandale, New Jersey 08801

Metal butterfly clusters that contain quadruply bridging oxo and sulfido ligands, [PPN][Fe₃M(CO)₁₂(μ_4-E)] (PPN = (PPh₃)₂N⁺, E = O, S; M = Mn, Re), were synthesized by condensation reactions between [PPN]₂[Fe₃(CO)₉-(μ_3-E)] (E = O, S) and the electrophilic reagents [Mn(CO)₃(NCCH₃)₃][PF₆] and Re(CO)₅(OSO₂CF₃). The structures of [PPN][Fe₃Mn(CO)₁₂(μ_4-O)] ([PPN]2) and [PPN][Fe₃Mn(CO)₁₂(μ_4-S)] ([PPN]5) were determined by single-crystal X-ray diffraction. The dihedral angle between the two wings of the butterfly is 113° for 2 and 130° for 5; presumably, this structural feature arises from the larger size of sulfur versus oxygen. The structure of 2 clearly indicates that the manganese atom occupies a wingtip site in the butterfly array of metal atoms. All of the butterfly clusters were characterized by variable-temperature ¹³C NMR spectroscopy and are assigned structures in which the heterometal occupies a wingtip site. Fenske–Hall molecular orbital calculations were performed on 2 and 5 as well as the parent trinuclear clusters. The electronic structures of [Fe₄(CO)₁₂(μ_4-C)]²⁻ and [Fe₄(CO)₁₂-(μ_4-N)]⁻, as indicated by Fenske–Hall calculations, are compared to those of 2 and 5 to assess the structural and electronic contributions of oxygen and sulfur to bonding within the butterfly framework. Crystal data for [PPN]-2: monoclinic ($P2_1/c$), a = 17.100(2) Å, b = 15.890(1) Å, c = 17.417(2) Å, β = 94.90(1)°, Z = 4, R (R_w) = 0.037 (0.044). Crystal data for [PPN]5: triclinic ($P\bar{1}$), a = 11.314(1) Å, b = 18.214(2) Å, c = 11.309(1) Å, α = 90.46(1)°, β = 90.22(1)°, γ = 89.43(1)°, Z = 2, R (R_w) = 0.037 (0.056).

Introduction

The coordination chemistry of cluster-bound carbide,[2] and nitride[3] ligands in metal carbonyl clusters has been extensively explored, and coordination environments that mimic the exposed environment characteristic of surfaces and the encapsulated environment characteristic of solid-state compounds have been

established. The variety of coordination environments established for other first-row main-group atoms is small. Recently, however, the more electron-rich and electron-poor main-group substituents oxygen[4,5] and boron,[6] respectively, have been characterized in a variety of new coordination environments, including the interesting μ_4-E "butterfly" clusters,[7] where the exposed ligand, E, is nestled between the wings of the butterfly (see I). The coordination environment of E in the butterfly

I
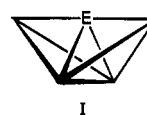
clusters has been proposed to model chemisorption on the steps of a metal surface.[7] The M₄-butterfly clusters with 5 metal–metal bonds and 62 cluster valence electrons (CVE) are intermediate in structure between M₄-tetrahedral clusters (6 M–M bonds, 60 CVE) and M₄-square planar clusters (4 M–M bonds, 64 CVE). Thus far, no examples of μ_4-E butterfly coordination of heavier (non-first-row) main-group atoms have been established for metal–carbonyl clusters.[8]

® Abstract published in *Advance ACS Abstracts*, March 15, 1995.

(1) (a) Northwestern University. (b) Current address: Department of Chemistry, The University of North Carolina, Chapel Hill, NC 27599-3290. (c) Exxon Research and Engineering Co.; Current address: Department of Chemistry, University of Wyoming, Laramie, WY 82071. (d) Current address: Department of Chemistry, The University of Virginia, Charlottesville, VA 22901. (e) Current address: Department of Chemistry, Southern Illinois University at Edwardsville, Edwardsville, IL 63026.

(2) (a) Muetterties, E. L.; Tachikawa, M. *Prog. Inorg. Chem.* **1981**, *28*, 203. (b) Bradley, J. S. *Adv. Organomet. Chem.* **1983**, *22*, 1.

(3) Gladfelter, W. L. *Adv. Organomet. Chem.* **1985**, *24*, 41.

(4) Schauer, C. K.; Shriver, D. F. *Angew. Chem., Int. Ed. Engl.* **1987**, *26*, 255. This reference contains ordering information for crystallographic data on [(PPh₃)₂N][Fe₃Mn(CO)₁₂(μ_4-O)].

(5) Square-planar μ_4-O clusters. (a) Schauer, C. K.; Voss, E. J.; Sabat, M.; Shriver, D. F. *J. Am. Chem. Soc.* **1989**, *111*, 7662. (b) Ingham, S. L.; Lewis, J.; Raithby, P. R. *J. Chem. Soc., Chem. Commun.* **1993**, 166.

(6) (a) Rath, N. P.; Fehlner, T. P. *J. Am. Chem. Soc.* **1987**, *109*, 5273. (b) Khattar, R.; Puga, J.; Fehlner, T. P.; Rheingold, A. L. *J. Am. Chem. Soc.* **1989**, *111*, 1877. (c) Hong, F.-E.; Coffy, T. J.; McCarthy, D. A.; Shore, S. G. *Inorg. Chem.* **1989**, *28*, 3284. (d) Harpp, K. S.; Housecroft, C. E.; Rheingold, A. L.; Shongwe, M. S. *J. Chem. Soc., Chem. Commun.* **1988**, 965. (e) Bandyopadhyay, A.; Shang, M.; Jun, C. S.; Fehlner, T. P. *Inorg. Chem.* **1994**, *33*, 3677. (f) Housecroft, C. E.; Matthews, D. M.; Rheingold, A. L.; Song, X. *J. Chem. Soc., Chem. Commun.* **1992**, 842. (g) Housecroft, C. E.; Matthews, D. M.; Rheingold, A. L. *Organometallics* **1992**, *11*, 2959. (h) Draper, S. M.; Housecroft, C. E.; Keep, A. K.; Matthews, D. M.; Song, X.; Rheingold, A. L. *J. Organomet. Chem.* **1992**, *423*, 241. (i) Chung, J.-H.; Knoeppel, D.; McCarthy, D.; Columbie, A.; Shore, S. G. *Inorg. Chem.* **1993**, *32*, 3391.

(7) Sappa, E.; Tiripicchio, A.; Carty, A. J.; Toogood, G. E. *Prog. Inorg. Chem.* **1987**, *35*, 437.

(8) A μ_4-S ligand bound to a butterfly arrangement of metal atoms has been observed in clusters with several sulfido ligands. See, for example (a) Curtis, M. D.; Williams, P. D. *Inorg. Chem.* **1983**, *22*, 2661. (b) Curtis, M. D.; Williams, P. D.; Butler, W. M. *Inorg. Chem.* **1988**, *27*, 2853. (c) Pasynskii, A. A.; Eremenko, I. L.; Ellert, O. G.; Novotortsev, V. M.; Rakitin, Y. V.; Kalinnikov, V. T.; Shklover, V. E.; Struchkov, Y. T. *J. Organomet. Chem.* **1982**, *234*, 315. (d) Eremenko, I. L.; Pasynskii, A. A.; Orazsakhatov, B.; Shestakov, A. F.; Gasanov, G. S.; Katugin, A. S.; Struchkov, Y. T.; Shklover, V. E. *J. Organomet. Chem.* **1988**, *338*, 369. (e) Ghilardi, C. A.; Midollini, S.; Sacconi, L. *J. Chem. Soc., Chem. Commun.* **1981**, 47.

This paper describes the synthesis, characterization, and bonding of butterfly clusters that contain μ_4-oxo and μ_4-sulfido atoms as ligands. The influence of the main-group atom and heterometal on the reactivity of these clusters will be described in subsequent papers.[9]

Experimental Section

Materials and General Procedures. All manipulations were performed under an atmosphere of prepurified, dry nitrogen by employing standard Schlenk and syringe techniques. Solids were manipulated in a Vacuum Atmospheres glovebox equipped with a recirculator and Dri-Train system. Solvents were distilled from the appropriate drying agent before use.[10] Bis(triphenylphosphine)nitrogen-(1+) chloride ([PPN]Cl) was purchased from Alfa Products and was used as received. The compounds [Mn(CO)$_3$(NCCH$_3$)$_3$][PF$_6$],[11] Re(CO)$_5$(OSO$_2$CF$_3$),[12] [PPN]$_2$[Fe$_3$(CO)$_{11}$],[13] and H$_2$Fe$_3$(CO)$_9$(μ_3-S)[14] were prepared by literature procedures, and [PPN]$_2$[Fe$_3$(CO)$_9$(μ_3-O)] was prepared by using a modification of a literature procedure[15] described below.

Infrared spectra were recorded on a Matteson Alpha Centauri spectrometer in solution using a CaF$_2$ windowed cell. Raman spectra were recorded on solid samples as previously described, utilizing 6764 Å Kr ion laser excitation.[16] ^{13}C NMR spectra were recorded on a JEOL FX-270 spectrometer (at 67.80 MHz) or a Varian XL-400 spectrometer (at 100.58 MHz), and the solvent resonance was used as an internal standard. Cr(acac)$_3$ (acac = acetylacetonate) was employed as a relaxation agent for all ^{13}C NMR samples. Elemental analyses were performed by Elbach Analytical Laboratories, Postfach 1315, D-5250 Engelskirchen, Germany.

Synthesis of [PPN]$_2$[Fe$_3$(CO)$_9$(μ_3-O)] ([PPN]1) and [PPN]$_2$[Fe$_3$-(*CO)$_9$ (μ_3-O)]. A sample of [PPN]$_2$[Fe$_3$(CO)$_{11}$] (5.0 g) was dissolved in 120 mL of acetone. Dry air was bubbled through the solution, and the formation of **1** was monitored by infrared spectroscopy. When the reaction was complete, the solution was purged with dry N$_2$ and filtered, and the volume was reduced to 15 mL. Addition of 10 mL of 2-propanol and further removal of solvent under vacuum led to a lightly colored supernatant and red crystals, which were isolated by filtration and were washed with 2-propanol (3 × 10 mL) followed by Et$_2$O (3 × 10 mL). Isolated yield: 3.5 g (70%). The ^{13}C-enriched oxo compound was prepared from [PPN]$_2$[Fe$_3$(*CO)$_{11}$].[17] ^{13}C NMR (acetone-d_6, δ): 223.4 (terminal CO's), ~130 (multiplet, [PPN]$^+$). Anal. Calcd (found) for C$_{81}$H$_{60}$N$_2$Fe$_3$O$_{10}$P$_4$: C, 64.31 (64.05); H, 4.00 (4.15); N, 1.85 (1.73); Fe, 11.07 (11.10).

Reaction of 1 with CO. A sample of **1** (70 mg) was placed in a 10 mm NMR tube equipped with a resealable valve. A portion of dry, degassed acetone-d_6 was distilled into the tube, and ^{13}CO (1.5 atm) was placed over the solution. The ^{13}C NMR spectrum of the solution was monitored periodically. After the sample was allowed to stand for 1 week, no starting cluster remained.

Synthesis of [PPN][Fe$_3$Mn(CO)$_{12}$(μ_4-O)] ([PPN]2). Samples of [Mn(CO)$_3$(NCCH$_3$)$_3$][PF$_6$] (0.280 g, 0.69 mmol) and [PPN]$_2$1 (1.000 g, 0.66 mmol) were dissolved in 30 mL of acetone, the mixture was stirred for 30 min and evaporated to dryness, and the cluster was extracted into Et$_2$O (20 mL). The solution was filtered, leaving behind [PPN][PF$_6$], and the filtrate was layered with pentane (30 mL). The

resulting brown-purple needlelike crystals were isolated by filtration and washed with pentane before drying under vacuum. Isolated yield: 0.530 g (75%). Anal. Calcd (found) for C$_{48}$H$_{30}$NFe$_3$MnO$_{13}$P$_2$: C, 51.79 (51.65); H, 2.72 (2.85); N, 1.26 (1.21); Fe, 15.05 (15.20); Mn, 4.94 (4.83).

Synthesis of [PPN][Fe$_3$Re(CO)$_{12}$(μ_4-O)] ([PPN]3). Samples of [Re-(CO)$_5$][SO$_3$CF$_3$] (0.110 g, 0.22 mmol) and [PPN]$_2$1 (0.300 g, 0.20 mmol) were dissolved in 5 mL of CH$_2$Cl$_2$, and an immediate color change to dark brown was observed. The solution was stirred for 12 h, and then the volume was reduced to 0.5 mL. Et$_2$O (10 mL) was added, and the solution was filtered, leaving behind [PPN][SO$_3$CF$_3$]. The volume of the filtrate was reduced to ~5 mL, and the solution was layered with pentane (10 mL). The brown needlelike crystals were isolated by filtration and washed with pentane before drying under vacuum. Isolated yield: 0.150 g (61%). Anal. Calcd (found) for C$_{48}$H$_{30}$NFe$_3$O$_{13}$P$_2$Re: C, 46.33 (46.19); H, 2.43 (2.39); N, 1.13 (1.30); Fe, 13.46 (12.90); Re, 14.96 (14.81).

Synthesis of [PPN]$_2$[Fe$_3$(CO)$_9$(μ_3-S)] ([PPN]$_2$4) and [PPN]$_2$[Fe$_3$-(*CO)$_9$(μ_3-S)]. A solution of KOH (0.120 g, 2.14 mmol) and [PPN]-Cl (1.250 g, 2.18 mmol) in MeOH (5 mL) was added to a solution of H$_2$Fe$_3$(CO)$_9$(μ_3-S) (0.450 g, 0.99 mmol) in 10 mL of pyridine. The solvent was removed under vacuum, and the cluster was extracted into CH$_2$Cl$_2$ (10 mL). The extract was then filtered, and the cluster was precipitated by addition of Et$_2$O. The isolated red/orange solid was washed thoroughly with Et$_2$O and then recrystallized from acetone/2-propanol. Isolated yield: 1.27 g (84%). Anal. Calcd (found) for C$_{81}$H$_{60}$N$_2$Fe$_3$O$_9$P$_4$S: C, 63.63 (63.00); H, 3.96 (4.10); N, 1.83 (1.78); S, 2.10 (1.93). [PPN]$_2$[Fe$_3$(*CO)$_9$(μ_3-S)] enriched with ^{13}CO at the carbonyl ligands (~30%) was prepared by vigorously stirring the pyridine/KOH mixture above (without [PPN]Cl) under 600 Torr of 99% ^{13}CO for 12 h. The ^{13}CO atmosphere above the solution was replaced twice, followed by 12 h of additional stirring after each replacement. This solution was transferred by cannula onto solid [PPN]Cl, and the workup was carried out as above.

Synthesis of [PPN][Fe$_3$Mn(CO)$_{12}$(μ_4-S)] ([PPN]5). Samples of [Mn(CO)$_3$(NCCH$_3$)$_3$][PF$_6$] (0.140 g, 0.34 mmol) and [PPN]$_2$4 (0.500 g, 0.33 mmol) were dissolved in 20 mL of acetone, and after 30 min of stirring, the solvent was removed. The cluster was extracted into Et$_2$O (10 mL), and the extract was filtered, leaving behind [PPN][PF$_6$]. Removal of the solvent under vacuum followed by extraction of the resulting oil with 2-propyl ether (5 mL) gave an oily suspension that crystallized upon standing. The brown crystals were washed with 2:1 (2-propyl ether/pentane), followed by pentane, before drying under vacuum. Isolated yield: 0.240 g (65%). Anal. Calcd (found) for C$_{48}$H$_{30}$NFe$_3$MnO$_{12}$P$_2$S: C, 51.05 (50.83); H, 2.68 (2.78); N, 1.24 (1.27); Fe, 14.84 (15.05); Mn, 4.86 (4.77); S, 2.84 (2.88).

Synthesis of [PPN][Fe$_3$Re(CO)$_{12}$(μ_4-S)] ([PPN]6). A sample of [PPN][Fe$_3$(CO)$_9$(μ_3-SRe(CO)$_5$)] (0.060 g, 0.046 mmol)[8b] was dissolved in 5 mL of 1,2 dichloroethane; the resulting solution was refluxed for 50 min and then filtered. The volume of the filtrate was reduced under vacuum to ~1 mL, and 3 mL of Et$_2$O was added before layering with pentane (10 mL). The black flaky crystals that separated from the solution were washed with pentane before drying under vacuum. Isolated yield: 0.050 g (87%). Anal. Calcd (found) for C$_{48}$H$_{30}$NFe$_3$ReO$_{12}$P$_2$S: C, 45.74 (45.78); H, 2.40 (2.39); N, 1.11 (1.12); Fe, 13.29 (13.69); Re, 14.77 (15.20); S, 2.54 (2.57).

X-ray Structure Determinations. For both [PPN]2 and [PPN]5, unit cell constant determination and data collection were performed on an Enraf-Nonius CAD4 diffractometer. Lattice parameters were determined by least-squares refinement of the setting angles of 25 high-angle reflections. The data collection was monitored by measurement of the intensities of four control reflections which showed no significant intensity variation over the course of data collection for either data set. During data reduction, Lorentz and polarization corrections were applied to the data. Neutral-atom scattering factors with anomalous scattering contributions[18] were utilized in all structure factor calculations. All computations were performed using the TEXSAN

(9) (a) Schauer, C. K.; Voss, E. J.; Sabat, M.; Stern, C. L.; Shriver, D. F. Manuscript in preparation. (b) Schauer, C. K.; Shriver, D. F. Manuscript in preparation.

(10) Gordon, A. J.; Ford, R. A. *The Chemist's Companion*; Wiley: New York, 1977.

(11) Drew, D.; Darensbourg, D. J.; Darensbourg, M. Y. *Inorg. Chem.* **1975**, *14*, 1579.

(12) Nitschke, J.; Schmidt, S. P.; Trogler, W. C. *Inorg. Chem.* **1985**, *24*, 1972.

(13) Hodali, H. A.; Shriver, D. F. *Inorg. Synth.* **1980**, *20*, 222.

(14) Markó, L.; Takács, J.; Papp, S.; Markó-Monostory, B. *Inorg. Chim. Acta* **1980**, *45*, L189.

(15) Ceriotti, A.; Resconi, L.; Demartin, F.; Longoni, G.; Manassero, M.; Sansoni, M. *J. Organomet. Chem.* **1983**, *249*, C35.

(16) Stanghellini, P. L.; Sailor, M. J.; Kuznesof, P.; Whitmire, K. H.; Hriljac, J. A.; Kolis, J. W.; Zheng, Y.; Shriver, D. F. *Inorg. Chem.* **1987**, *26*, 2950.

(17) Hriljac, J. A.; Shriver, D. F. *J. Am. Chem. Soc.* **1987**, *109*, 6010.

(18) *International Tables for X-ray Crystallography*; Kynoch Press: Birmingham, England, 1974; Vol. IV, pp 99, 149.

Table 1. Crystallographic Data for [PPN][Fe$_3$Mn(CO)$_{12}$(μ_4-O)] and [PPN][Fe$_3$Mn(CO)$_{12}$(μ_4-S)]

	[PPN][Fe$_3$Mn(CO)$_{12}$(μ_4-O)], [PPN]**2**	[PPN][Fe$_3$Mn(CO)$_{12}$(μ_4-S)], [PPN]**5**
formula	C$_{48}$H$_{30}$Fe$_3$MnNO$_{13}$P$_2$	C$_{48}$H$_{30}$Fe$_3$MnNO$_{12}$P$_2$S
fw	1112.92	1129.25
temp, °C	−120	−120
space group	$P2_1/c$ (No. 14)	$P\bar{1}$ (No. 2)
a, Å	17.100(2)	11.314(1)
b, Å	15.890(1)	18.214(2)
c, Å	17.417(2)	11.309(1)
α, deg		90.46(1)
β, deg	94.90(1)	90.22(1)
γ, deg		89.43(1)
V, Å^3	4715(2)	2330.3(7)
Z	4	2
$R(F)^a$	0.037	0.037
$R_w(F)^b$	0.044	0.056
ϱ_{calc}, g cm^{-3}	1.57	1.61
μ(Mo Kα), cm^{-1}	13.38	13.95
λ, Å	0.710 69	0.710 69

^{a} $R(F) = (\sum||F_o| - |F_c||)/\sum|F_o|$. ^{b} $R_w(F) = [(\sum w(|F_o| - |F_c|)^2)/\sum wF_o^2]^{1/2}$; $w = 4F_o^2/\sigma^2(F_o^2)$.

crystallographic computing package[19] on a VAX 11/730 computer. Least-squares refinement on F minimized the function $\sum w(|F_o| - |F_c|)^2$.

Structure Determination for [PPN]2. Crystals suitable for study by X-ray diffraction were grown by slow diffusion of pentane into an ether solution of [PPN]**2**. Crystal data for [PPN]**2**, together with details of the X-ray diffraction experiment and subsequent computations, are shown in Table 1. No absorption correction was performed due to the small average value of μt. The space group was unambiguously determined to be $P2_1/c$ from the systematic absences. The structure was solved by the direct-method routine MITHRIL,[20] which revealed the metal atom positions. Subsequent Fourier difference maps revealed the positions of all remaining atoms, including the hydrogen atoms of the [PPN]$^+$ cation. One of the metal atoms was assigned as Mn on the basis of the observed structural parameters (see discussion below). The final structural model utilized anisotropic thermal parameters for all non-hydrogen atoms and included the hydrogen atoms as fixed contributors to the structure factors. The largest peak in the final difference map ($\sim$1 e Å^{-3}) was located near the metal atoms.

Final fractional atomic coordinates and equivalent isotropic thermal parameters for the cluster anion **2** may be found in Table 2. Bond lengths and bond angles relevant to the cluster anion are displayed in Table 3.

Structure Determination for [PPN]5. Crystals suitable for study by X-ray diffraction were obtained in a typical preparation of [PPN]**5** (see above). Crystal data, together with details of the X-ray diffraction experiment and subsequent computations, are shown in Table 1. Although the unit cell parameters are suggestive of a tetragonal unit cell, careful examination of the axial photographs indicated the requisite symmetry was not present; thus the structure was solved and refined in the triclinic space group, $P\bar{1}$. An empirical absorption correction was applied to the raw data, utilizing the intensity profiles for six reflections as a function of ψ. The range of transmission factors for the complete data set was $\pm4\%$ of the mean value. The structure was solved by the direct-methods routines of the SHELXS-86 package.[21] Subsequent calculations were performed with the TEXSAN structure determination package.[19]

One of the wingtip metal atoms was arbitrarily assigned as manganese. The refined structural parameters indicated the presence of a noncrystallographic 2-fold axis passing through S and the center

(19) *TEXSAN*, Version 2.0; Molecular Structure Corp.: College Station, TX, 1987.
(20) Gilmore, G. J. *J. Appl. Crystallogr.* **1984**, *17*, 42.
(21) Sheldrick, G. SHELXS-86. George Sheldrick, University of Göttingen, 1986.

Table 2. Fractional Atomic Coordinates for the Cluster Anion **2** in [PPN][Fe$_3$Mn(CO)$_{12}$(μ_4-O)]

atom	x	y	z
Fe1	0.2710(3)	0.20666(3)	0.40313(3)
Fe2	0.18324(3)	0.19309(3)	0.51004(3)
Fe3	0.14590(3)	0.29051(3)	0.39884(3)
Mn1	0.32194(3)	0.26308(4)	0.53839(3)
O1	0.2339(1)	0.2886(1)	0.4706(1)
O2	0.4073(2)	0.0997(2)	0.4445(2)
O3	0.3475(2)	0.3057(2)	0.2874(2)
O4	0.2038(2)	0.0685(2)	0.3083(2)
O5	0.2644(2)	0.0718(2)	0.6155(2)
O6	0.0805(2)	0.2596(2)	0.6237(2)
O7	0.0805(2)	0.0627(2)	0.4385(2)
O8	0.1816(2)	0.4193(2)	0.2852(2)
O9	0.0396(2)	0.1907(2)	0.2946(2)
O10	0.0201(2)	0.3790(2)	0.4702(2)
O11	0.4506(2)	0.3741(2)	0.4995(2)
O12	0.4368(2)	0.1553(2)	0.6280(2)
O13	0.2971(3)	0.3612(2)	0.6766(2)
C2	0.3549(2)	0.1462(3)	0.4354(2)
C3	0.3175(3)	0.2681(3)	0.3325(3)
C4	0.2295(2)	0.1245(3)	0.3440(3)
C5	0.2385(2)	0.1236(3)	0.5743(3)
C6	0.1209(3)	0.2351(3)	0.5788(3)
C7	0.1202(2)	0.1151(3)	0.4658(3)
C8	0.1684(2)	0.3693(3)	0.3293(3)
C9	0.0815(3)	0.2300(2)	0.3352(3)
C10	0.0690(2)	0.3451(3)	0.4421(3)
C11	0.3997(3)	0.3307(3)	0.5146(3)
C12	0.3917(2)	0.1981(3)	0.5927(3)
C13	0.3061(3)	0.3224(3)	0.6226(3)

Table 3. Intramolecular Distances (Å) and Angles (deg) for the Cluster Anion **2** in [PPN][Fe$_3$Mn(CO)$_{12}$(μ_4-O)]^a

Distances			
Fe1−O1	1.899(2)	Fe1−Mn1	2.6002(9)
Fe2−O1	1.904(2)	Fe2−Fe3	2.5187(8)
Fe3−O1	1.872(3)	Fe2−Mn1	2.6280(9)
Mn1−O1	1.877(3)	Fe−C(av)^b	1.788(13)
Fe1−Fe2	2.4990(8)	Mn−C(av)^b	1.785(2)
Fe1−Fe3	2.5161(8)	C−O(av)^b	1.151(8)

Angles			
O1−Fe1−Fe2	49.00(7)	Fe3−O1−Mn1	168.3(1)
O1−Fe1−Fe3	47.70(8)	Fe3−O1−Fe1	83.7(1)
O1−Fe1−Mn1	46.11(8)	Fe3−O1−Fe2	83.7(1)
Fe−Fe1−Fe3	60.29(2)	Mn1−O1−Fe1	87.0(1)
Fe2−Fe1−Mn1	62.01(2)	Mn1−O1−Fe2	88.1(1)
Fe3−Fe1−Mn1	93.58(3)	Fe1−O1−Fe2	82.2(1)
O1−Fe2−Fe1	48.84(7)	O2−C2−Fe1	168.3(4)
O1−Fe2−Fe3	47.63(8)	O3−C3−Fe1	178.8(4)
O1−Fe2−Mn1	45.53(8)	O4−C4−Fe1	176.8(5)
Fe1−Fe2−Fe3	60.19(2)	O5−C5−Fe2	170.1(4)
Fe1−Fe2−Mn1	60.89(2)	O6−C6−Fe2	177.9(4)
Fe3−Fe2−Mn1	92.85(3)	O7−C7−Fe2	177.9(4)
O1−Fe3−Fe1	48.61(7	O8−C8−Fe3	179.2(4)
O1−Fe3−Fe2	48.70(7)	O9−C9−Fe3	179.4(5)
Fe1−Fe3−Fe2	59.52(2)	O10−C10−Fe3	179.1(4)
O1−Mn1−Fe1	46.84(7)	O11−C11−Mn1	179.4(4)
O1−Mn1−Fe2	46.39(7)	O12−C12−Mn1	179.5(4)
Fe1−Mn1−Fe2	57.10(2)	O13−C13−Mn1	178.8(5)

^{a} Estimated standard deviations in the least significant figure are given in parentheses. ^{b} For average distances, root-mean-square estimated standard deviations are reported.

of the Fe1−Fe2 bond, suggesting that the manganese atom is disordered among the wingtip metal atoms. The final structural model utilized anisotropic thermal parameters on all non-hydrogen atoms except the carbon atoms of the phenyl groups in the [PPN]$^+$ cation. Hydrogen atoms were located in the Fourier difference maps, and they were included as fixed contributors to the structure factors. The largest peak in the final difference map ($\sim$0.8 e Å^{-3}) was located near one of the phenyl rings.

Table 4. Fractional Atomic Coordinates for the Cluster Anion **5** in [PPN][Fe₃Mn(CO)₁₂(μ_4-S)]

atom	x	y	z
Fe1	−0.04058(5)	0.27907(4)	0.10583(5)
Fe2	0.10584(5)	0.22097(4)	−0.04061(5)
Fe3	0.03579(6)	0.14629(4)	0.13927(6)
Mn	0.13922(6)	0.35372(4)	0.03584(6)
S	0.1462(1)	0.24995(6)	0.1463(1)
O2	−0.1450(3)	0.4061(2)	−0.0099(3)
O3	−0.1473(3)	0.3167(3)	0.3336(3)
O4	−0.2394(3)	0.1991(2)	0.0060(4)
O5	0.0062(4)	0.3006(2)	−0.2396(3)
O6	0.3328(3)	0.1826(3)	−0.1469(3)
O7	−0.0097(3)	0.0935(2)	−0.1449(3)
O8	−0.0427(4)	0.1437(2)	0.3856(4)
O9	−0.1404(3)	0.0355(2)	0.0761(3)
O10	0.2243(3)	0.0353(2)	0.1601(3)
O11	0.1603(3)	0.4648(2)	0.2243(3)
O12	0.0757(3)	0.4643(2)	−0.1398(3)
O13	0.3849(3)	0.3565(2)	−0.0424(4)
C2	−0.0902(4)	0.3601(3)	0.0337(4)
C3	−0.1033(4)	0.3022(3)	0.2447(4)
C4	−0.1576(4)	0.2261(3)	0.0484(5)
C5	0.0482(5)	0.2745(3)	−0.1571(5)
C6	0.2451(4)	0.1975(3)	−0.1032(4)
C7	0.0334(4)	0.1397(3)	−0.0905(4)
C8	−0.0098(5)	0.1445(3)	0.2894(5)
C9	−0.0716(4)	0.0799(3)	0.0999(4)
C10	0.1514(5)	0.0777(3)	0.1516(4)
C11	0.1513(4)	0.4221(3)	0.1506(5)
C12	0.1002(4)	0.4202(3)	−0.0713(4)
C13	0.2891(5)	0.3553(3)	−0.0097(5)

Table 5. Intramolecular Distances (Å) and Angles (deg) for the Cluster Anion **5** in [PPN][Fe₃Mn(CO)₁₂(μ_4-S)][a]

Distances			
Fe1−S	2.221(1)	Fe1−Mn	2.588(1)
Fe2−S	2.222(1)	Fe2−Fe3	2.587(1)
Fe3−S	2.275(1)	Fe2−Mn	2.592(1)
Mn−S	2.274(1)	Fe−C(av)[b]	1.778(12)
Fe1−Fe2	2.562(1)	Mn−C(av)[b]	1.781(14)
Fe1−Fe3	2.590(1)	C−O(av)[b]	1.147(7)

Angles			
S−Fe1−Fe2	54.79(3)	Fe1−S−Mn	70.29(4)
S−Fe1−Mn	55.82(4)	Fe1−S−Fe3	70.34(4)
S−Fe1−Fe3	55.81(4)	Fe2−S−Mn	70.41(4)
Fe2−Fe1−Mn	60.43(3)	Fe2−S−Fe3	70.25(4)
Fe2−Fe1−Fe3	60.29(3)	Mn−S−Fe3	131.31(5)
Mn−Fe1−Fe3	106.35(3)	O2−C2−Fe1	165.7(4)
S−Fe2−Fe1	54.76(3)	O3−C3−Fe1	178.0(5)
S−Fe2−Fe3	55.85(4)	O4−C4−Fe1	172.0(5)
S−Fe2−Mn	55.75(4)	O4−C4−Fe3	123.7(4)
Fe1−Fe2−Fe3	60.39(3)	O5−C5−Fe2	170.9(4)
Fe1−Fe2−Mn	60.28(3)	O6−C6−Fe2	177.8(4)
Fe3−Fe2−Mn	106.31(3)	O7−C7−Fe2	166.0(4)
S−Fe3−Fe2	53.91(3)	O8−C8−Fe3	178.0(5)
S−Fe3−Fe1	53.85(3)	O9−C9−Fe3	178.4(4)
Fe2−Fe3−Fe1	59.32(3)	O10−C10−Fe3	179.3(5)
S−Mn−Fe1	53.88(3)	O11−C11−Mn	178.9(5)
S−Mn−Fe1	53.84(3)	O12−C12−Mn	178.9(4)
Fe1−Mn−Fe2	59.29(3)	O13−C13−Mn	178.1(5)
Fe1−S−Fe2	70.45(4)		

[a] Estimated standard deviations in the least significant figure are given in parentheses. [b] For average distances, root-mean-square estimated standard deviations are reported.

Final fractional atomic coordinates and equivalent isotropic thermal parameters for the cluster anion **5** may be found in Table 4. Bond lengths and angles relevant to the cluster anion are displayed in Table 5.
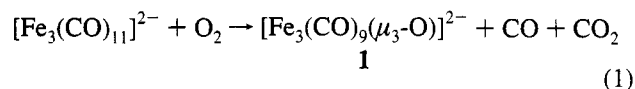
Calculational Details. All of the theoretical results were obtained by Fenske−Hall molecular orbital calculations.[22] The 1s through 3d

(22) Hall, M. B.; Fenske, R. F. *Inorg. Chem.* **1972**, *11*, 768.

functions for Mn and Fe were taken from Richardson et al.,[23] while the 4s and 4p were chosen to have exponents of 2.0. The carbon, oxygen, and sulfur functions were taken from the double-ζ functions of Clementi.[24] The valence p functions were retained as the double-ζ functions, while all other functions were reduced to single-ζ form. In the calculations for **2** and **5**, the local coordinate system on the oxygen or sulfur atom was oriented with the x axis parallel to a line connecting the two hinge atoms, the y axis parallel to a line connecting the two wingtip iron atoms, and the z axis pointing out of the cluster.

The reported atomic positions[25] of the anion **4** were idealized to give a cluster having C_{3v} symmetry. Although the structure of anion **1** has been reported,[15] the atomic coordinates were not available, so a Fe₃O framework of C_{3v} symmetry was constructed from the reported core bond distances and angles. The Fe(CO)₃ groups were positioned so that the "equatorial" CO ligands are tilted up out of the Fe₃ plane by 29°; this is the angle observed in [Co₃(CO)₉(μ_3-CCH₃)],[26] a cluster in which the Co−Co and Co−C distances are nearly identical to the Fe−Fe and Fe−O distances in anion **1**. The distances and angles within the Fe(CO)₃ group were taken to be identical to those in anion **4**. The atomic positions for **2** reported herein were idealized to give a cluster having C_s symmetry. Calculations were carried out for **5** using the atomic positions reported in this paper idealized to C_2 symmetry, as well as for a modified structure described later in the paper.

Results and Discussion

Synthesis and Reactivity of [Fe₃(CO)₉(μ_3-E)]²⁻ Clusters (E = O, S). The clusters [PPN]₂[Fe₃(CO)₉(μ_3-O)] (**1**) and [PPN]₂[Fe₃(CO)₉(μ_3-S)] (**4**) were utilized as the precursors to four-metal oxo and sulfido clusters. The anion of the oxo cluster, **1**, was originally prepared by Ceriotti et al. as the [BzMe₃N]⁺ salt by oxidation of [Fe₃(CO)₁₁]²⁻ (eq 1).[15] This

$$[\text{Fe}_3(\text{CO})_{11}]^{2-} + \text{O}_2 \rightarrow [\text{Fe}_3(\text{CO})_9(\mu_3\text{-O})]^{2-} + \text{CO} + \text{CO}_2$$
$$\mathbf{1}$$

(1)

synthesis is a rare example of a high-yield reaction of a cluster with O₂. Deprotonation of H₂Fe₃(CO)₉(μ_3-S), which is prepared by acidification of a methanolic solution containing HFe(CO)₄⁻ and Na₂S·9H₂O,[14] gives the sulfido cluster, **4**, in high yield.

The nature of the heteroatom in the trinuclear clusters, **1** and **4**, strongly influences the cluster reactivity. The oxo cluster, **1**, reacts with proton sources at the oxygen atom to yield a hydroxyl capped cluster (eq 2),[15] whereas the sulfido cluster, **4**, protonates on a metal−metal bond (eq 3).[14] The orbital
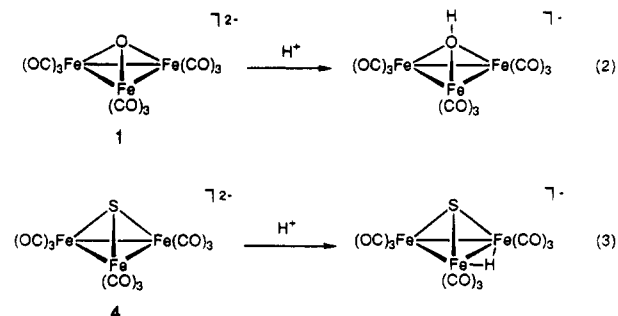
structures of **1** and **4** are very similar (see below) and thus do not offer an explanation for these differences in reactivity; the

(23) Richardson, J. W.; Nieupoort, W. C.; Powell, R. R.; Edgell, W. F. *J. Chem. Phys.* **1962**, *36*, 1057.

(24) Clementi, E. *J. Chem. Phys.* **1964**, *40*, 1944.

(25) Al-ani, F. T.; Hughes, D. L.; Pickett, C. J. *J. Organomet. Chem.* **1986**, *307*, C31.

(26) Sutton, P. W.; Dahl, L. F. *J. Am. Chem. Soc.* **1967**, *89*, 261.

Table 6. Properties of $[Fe_3(CO)_9(\mu_3\text{-E})]^{2-}$ Clusters (E = O, S)

	$[Fe_3(CO)_9(\mu_3\text{-O})]^{2-}$ (1)	$[Fe_3(CO)_9(\mu_3\text{-S})]^{2-}$ (4)
IR (V_{CO}, cm^{-1})	2000 w, 1928 vs, 1899 s, 1869 m^a	1997 w, 1927 vs, 1901 s, 1870 m^a
^{13}C NMR (δ, ppm)	223.5^b	223.9^b
Raman (M$-$M, cm^{-1})	240, 194	214, 176
Fe$-$Fe$_{av}$ (Å)	2.49^c	2.59^d
Fe$-$E$_{av}$ (Å)	1.89^c	2.19^d

^{a} [PPN]$^+$ salt in acetone. Key: vs = very strong; s = strong; m medium; w = weak. ^{b} [PPN]$^+$ salt in acetone-d_6. ^{c} Reference 15. ^{d} Reference 25.

Table 7. Overlap Populations in $[Fe_3(CO)_9(\mu_3\text{-E})]^{2-}$ Clusters (E = O, S)^a

	$[Fe_3(CO)_9(\mu_3\text{-O})]^{2-}$ (1)	$[Fe_3(CO)_9(\mu_3\text{-S})]^{2-}$ (4)
	Fe$-$Fe	
d$-$d	0.016	0.014
total (d,s,p)	0.056	0.055
	E$-$Fe	
E(p$_x$, p$_y$)$-$Fe(d,s,p)	0.135	0.121
E(p$_z$)$-$Fe(d,s,p)	0.035	0.053
total	0.170	0.174

^{a} The local coordinate system on the bridging ligands is defined so the z axis is perpendicular to the Fe$_3$ plane while the x and y axes lie in a plane parallel to the Fe$_3$ plane.

nature of the higher energy orbitals suggests that a proton would initially attack the metal framework in either cluster. The identity of the final product is likely governed by the relative strength of O$-$H bonds (111 kcal mol^{-1} in H_2O) versus S$-$H bonds (88 kcal mol^{-1} in H_2S).

During an attempt to exchange normal isotopic **1** with ^{13}CO, it was discovered that the oxo ligand reacts readily with carbon monoxide at room temperature to generate CO_2 and lower nuclearity iron compounds (eq 4). This decomposition was
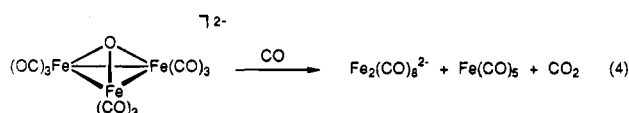
monitored by ^{13}C NMR spectroscopy under ^{13}CO in acetone-d_6 solution. Signals were observed for *CO_2 (at δ 125.7) and Fe(*CO)$_5$ (δ 221.4); orange crystals of [PPN]$_2$[Fe$_2$(*CO)$_8$] precipitated from solution over the course of the reaction. The corresponding binary metal$-$carbonyl cluster, [PPN]$_2$[Fe$_3$-(CO)$_{11}$], also decomposes under CO to give Fe(CO)$_5$ and [PPN]$_2$[Fe$_2$(CO)$_8$].[27] It is not clear whether loss of the oxo ligand (eq 4) occurs prior to or simultaneous with the cluster degradation. In contrast, the sulfido cluster, **5**, is quite stable to a carbon monoxide atmosphere.

Properties and Bonding of $[Fe_3(CO)_9(\mu_3\text{-E})]^{2-}$ Clusters (E = O, S). These trinuclear iron clusters differ only in the identity of the capping atom. A change in the capping atom from oxygen to sulfur, a much larger and less electronegative element (r(cov,O) = 0.73 Å, χ(O) = 3.50; r(cov,S) = 1.02 Å, χ(S) = 2.44), might be expected to have a significant influence on the structural and spectroscopic properties of the trinuclear cluster. Data comparing these properties are summarized in Table 6. The structures of the two clusters reflect the difference in size of the oxygen and sulfur atoms. The difference in the average Fe$-$E distance observed for **1** and **4** is compatible with the difference in covalent radii for oxygen and sulfur. The longer Fe$-$Fe distances in **4** are also a consequence of the large size of sulfur. A correlation has been developed between the metal$-$metal bond distances and the size of bridging atoms in dinuclear compounds.[28,29]

Surprisingly, the infrared spectra in the CO stretching region and the ^{13}C NMR chemical shifts for the CO ligands are nearly identical for **1** and **4**, Table 6. The bonding in the cluster framework was probed by examination of the symmetric and antisymmetric Fe$-$Fe stretching modes. Raman data, Table 6, reveal that these modes are on average approximately 20 cm^{-1}

higher in energy in the oxo cluster than in the sulfido cluster.

To better understand the similarities and differences in the two cluster, Fenske$-$Hall molecular orbital calculations were carried out for both **1** and **4**. The bonding in Co$_3$(CO)$_9$(μ_3-S) and related clusters has been discussed in some detail,[30,31] so the discussion here focuses on the effect of varying the μ_3-bridging ligand. The calculated charge distributions and overlap populations for **1** and **4** are very similar. The O atom in **1** is calculated to be slightly more negative than the S atom in **4** (-0.486 vs -0.431). The Fe atoms in both clusters carry nearly equal small charges (-0.015 in **1** vs -0.022 in **4**). The shift of charge toward O is consistent with the relative electronegativities of O and S, but it is smaller than might be expected. It is not surprising, in light of the similar charge distributions in the Fe$_3$E framework of the two clusters, that the charge distributions on the CO ligands are also very similar. When the results of the calculations are interpreted in terms of the CO ligand orbitals, the 5σ and 2π orbital populations on comparable CO ligands in clusters **1** and **4** are almost identical. This fact is consistent with the very similar stretching frequencies and ^{13}C chemical shifts for the CO ligands in the two clusters. The Fe$-$Fe and Fe$-$E overlap populations are listed in Table 7. Although the total Fe$-$S and Fe$-$O overlap populations are very similar, a comparison of the values for the individual S and O orbitals reveals differences between the Fe$-$O and Fe$-$S bonding interactions. More of the net M$-$S bonding in **4** occurs through the π-type orbitals (p$_x$$-p_y$) of S than through the σ-type (p$_z$) orbital, as previously observed for Co$_3$(CO)$_9$(μ_3-S) and related clusters.[30,31] This trend is reflected in larger M$-$S overlap populations for the sulfur π(p$_x$$-p_y$) orbitals compared to the sulfur σ(p$_z$) orbital. The contribution of the oxygen σ-(p$_z$) orbital to the total Fe$-$O bonding in **1** is even less (O(p$_z$)$-$Fe(d,s,p) = 0.035, S(p$_z$)$-$Fe(d,s,p) = 0.053). The total Fe$-$Fe overlap populations for **1** and **4** are very similar. Despite the fact that the Fe$-$Fe distances in **1** are nearly 0.1 Å shorter, the d$-$d overlap populations are only slightly larger.

The similarities between these two clusters suggest that the Fe$_3$(CO)$_9$ framework can readily adjust to accommodate the different bridging ligands with fairly small perturbations of the overall cluster bonding. The differently sized O and S atoms can be accommodated by changes in the metal$-$ligand and metal$-$metal bond distances, as well as reorientation of the Fe-(CO)$_3$ groups. This expansion and reorientation appear to optimize both the bonding between the triply bridging atom and the metal framework and the bonding within the metal framework itself.

Synthesis of Four-Metal Oxo Clusters. Although there are numerous examples of polyoxometalates[32] and organometallic

(27) Stanton Ching, private communication.
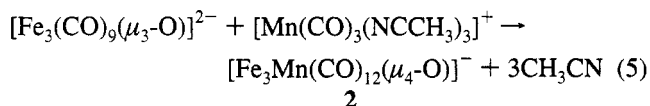(28) Dahl, L. F.; deGil, E. R.; Feltham, R. D. *J. Am. Chem. Soc.* **1969**, *91*, 1653.
(29) Dahl, L. F.; Costello, W. R.; King, R. B. *J. Am. Chem. Soc.* **1968**, *90*, 5422.

(30) Schilling, B. E. R.; Hoffmann, R. *J. Am. Chem. Soc.* **1979**, *101*, 3456.
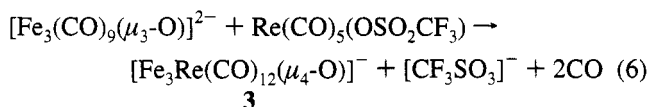(31) Chesky, P. T.; Hall, M. B. *Inorg. Chem.* **1983**, *22*, 2998.

oxo clusters[33] that contain metals in high oxidation states, the synthesis and chemistry of clusters comprised of low oxidation state metals that contain an oxo ligand are not very well developed. There are only a few examples of low-valent clusters which contain a μ_3-oxo ligand,[15,34,35] and the triiron cluster, **1**, is one of the very few that can be synthesized in good yield.

The facility of oxygen atom transfer to CO for **1** (see above) had to be taken into account in choosing cluster-building reagents. In reactions of **1** with reagents such as $Fe_2(CO)_9$, where carbon monoxide is liberated over the course of the reaction, the primary reaction products did not contain an oxo ligand. The cationic species $[Mn(CO)_3(NCCH_3)_3][PF_6]$ is a convenient reagent to deliver an $[M(CO)_3]^+$ fragment, without CO evolution. Reactions of **1** with 1 equiv of $[Mn(CO)_3(NCCH_3)_3]^+$ proceed smoothly in acetone solution to generate the four-metal oxo cluster in good yield (eq 5).

$$[Fe_3(CO)_9(\mu_3\text{-}O)]^{2-} + [Mn(CO)_3(NCCH_3)_3]^+ \rightarrow$$
$$\underset{\textbf{2}}{[Fe_3Mn(CO)_{12}(\mu_4\text{-}O)]^-} + 3CH_3CN \quad (5)$$

Formation of the product can be readily monitored by infrared spectroscopy, where the most intense CO stretching band shifts by ~50 cm^{-1} to higher energy (Table 8).

Reaction between **1** and the rhenium reagent $Re(CO)_5(OSO_2\text{-}CF_3)$[12] proceeds instantaneously in CH_2Cl_2 solution to yield an intermediate oxo–Fe_3Re cluster. Carbon monoxide loss from the intermediate cluster occurs over a period of several hours to generate the four-metal oxo cluster (eq 6).

$$[Fe_3(CO)_9(\mu_3\text{-}O)]^{2-} + Re(CO)_5(OSO_2CF_3) \rightarrow$$
$$\underset{\textbf{3}}{[Fe_3Re(CO)_{12}(\mu_4\text{-}O)]^-} + [CF_3SO_3]^- + 2CO \quad (6)$$

The intermediate cluster is stable to a carbon monoxide atmosphere since evolution of CO during the course of the reaction does not result in degradation of the product. The pattern observed in the infrared CO stretches for the Fe$_3$MnO$^-$ and Fe$_3$ReO$^-$ clusters is very similar (see Table 8), implying that the products are isostructural. Unlike the parent M_3O cluster (**1**), the oxo clusters, **2** and **3**, are not prone to lose the oxo ligand as CO_2 under a CO atmosphere.

Possible Structures and Electron Counts. There are two structural possibilities for the four-metal products of formulation $[Fe_3M(CO)_{12}(O)]^-$ obtained in these reactions (see **II** and **III**). The number of electrons donated to the cluster by the oxo ligand depends on the disposition of metal atoms about the ligand. If the oxo ligand caps a face of a tetrahedral cluster as in **II**, one orbital oriented away from the cluster contains a lone pair so

II   III

the oxo ligand donates four electrons to yield an electron-precise (60 CVE) tetrahedral cluster. If the oxo ligand binds to all four metal atoms disposed in a butterfly arrangement as in **III**, it may donate six electrons to give the expected 62 CVE of a butterfly cluster.

Structure of $[PPN][Fe_3Mn(CO)_{12}(\mu_4\text{-}O)]$, $[PPN]2$. The formulation of **2** as a butterfly oxo cluster was established by

2, M = Mn

3, M = Re
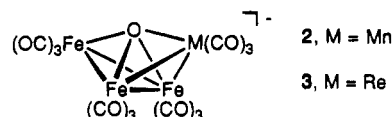
single-crystal X-ray diffraction, Figure 1. This complex appears to be a rare example of a mixed-metal cluster that crystallizes with no sign of disorder among the metal atom types. The three metal–metal distances involving the two hinge metal atoms (M_h, Fe1 and Fe2) and one of the wingtip metal atoms (M_w, Fe3) in **2** are nearly equivalent and are approximately equal to the Fe–Fe distances observed in the parent triiron oxo cluster, **1**. The remaining wingtip metal atom, which binds to the two hinge metal atoms at distances that are approximately 0.1 Å longer than the other metal–metal distances, is assigned as manganese. The assignment of manganese to a wingtip position in the butterfly is consistent with the variable-temperature ^{13}C NMR spectra (see below). The metal–metal bonding patterns in **2** are quite distinct from the bonding in the homometallic tetrairon clusters $[Fe_4(CO)_{12}(\mu_4\text{-}C)]^{2-}$ (**7**)[36] and $[Fe_4(CO)_{12}(\mu_4\text{-}N)]^-$ (**8**),[37] where the M_h–M_h distance is considerably shorter than the M_h–M_w distances.

The disposition of the array of carbon monoxide ligands about the triiron portion of **2** is largely unperturbed from that observed for the parent cluster, **1**. A comparison of the side views of **2** and the carbide cluster, **7** (**IV** and **V**, respectively), shows that
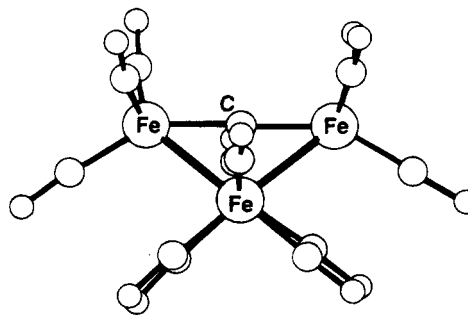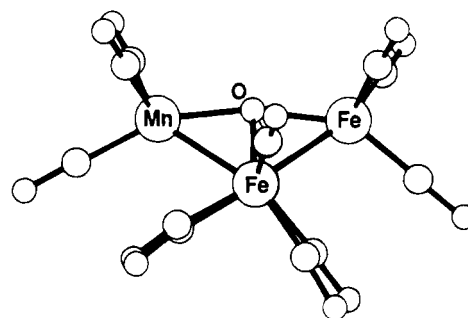
(32) Pope, M. T. *Heteropoly and Isopoly Oxometalates*; Springer-Verlag: Berlin, 1983.

(33) Bottomley, F.; Sutin, L. *Adv. Organomet. Chem.* **1988**, *28*, 339.

(34) (a) Uchtman, V. A.; Dahl, L. F. *J. Am. Chem. Soc.* **1969**, *91*, 3763. (b) Bertolucci, A.; Freni, M.; Romiti, P.; Ciani, G.; Sironi, A.; Albano, V. G. *J. Organomet. Chem.* **1976**, *113*, C61. (c) Lavigne, G.; Lugan, N.; Bonnet, J.-J. *Nouv. J. Chim.* **1981**, *5*, 423. (d) Goudsmit, R. J.; Johnson, B. F. G.; Lewis, J.; Raithby, P. R.; Whitmire, K. H. *J. Chem. Soc., Chem. Commun.* **1983**, 246. (e) Colombié, A.; Bonnet, J.-J.; Fompeyrine, P.; Lavigne, G.; Sunshine, S. *Organometallics* **1986**, *5*, 1154. (f) Gibson, C. P.; Huang, J.-S.; Dahl, L. F. *Organometallics* **1986**, *5*, 1676. (g) Gibson, C. P.; Rae, A. D.; Tomchick, D. R.; Dahl, L. F. *J. Organomet. Chem.* **1988**, *340*, C23.

(35) A series of oxo clusters prepared from oxidation of a Re(CO)$_3$ fragment in mixed-metal Pt$_3$Re clusters have been recently reported. (a) Xiao, J.; Vittal, J. J.; Puddephatt, R. J.; Manojlovíc-Muir, L.; Muir, K. W. *J. Am. Chem. Soc.* **1993**, *115*, 7882. (b) Xiao, J.; Puddephatt, R. J.; Manojlovíc-Muir, L.; Muir, K. W.; Torabi, A. A. *J. Am. Chem. Soc.* **1994**, *116*, 1129. (c) Hao, L.; Xiao, J.; Vittal, J. J.; Puddephatt, R. J. *Angew. Chem., Int. Ed. Engl.* **1995**, *34*, 346. (d) Xiao, J.; Hao, L.; Puddephatt, R. J.; Manojlovíc-Muir, L.; Muir, K. W. *J. Am. Chem. Soc.* **1995**, *117*, 6316.

IV

V

Table 8. Infrared CO Stretching Frequencies of Butterfly Oxo and Sulfido Clusters[a]

anion	ν_{CO}, cm^{-1}
$[Fe_3Mn(CO)_{12}(\mu_4\text{-O})]^-$ (2)	2055 vw, 2005 s, 1986 vs, 1961 w, 1943 mw, 1918 vw
$[Fe_3Re(CO)_{12}(\mu_4\text{-O})]^-$ (3)	2056 vw, 2011 s, 1990 vs, 1967 m, sh, 1928 m, 1905 w
$[Fe_3Mn(CO)_{12}(\mu_4\text{-S})]^-$ (5)	2056 vw, 2007 s, 1984 vs, 1966 m, sh, 1937 m, 1882 vw
$[Fe_3Re(CO)_{12}(\mu_4\text{-S})]^-$ (6)	2057 vw, 2014 s, 1988 s, 1975 m, sh, 1923 m, 1875 vw

[a] [PPN]$^+$ salt in CH_2Cl_2. Key: vs = very strong; s = strong; m = medium; w = weak; vw = very weak; sh = shoulder.
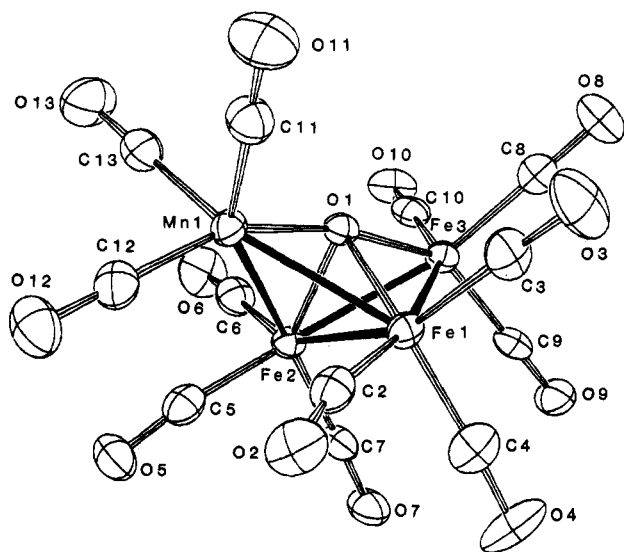
Figure 1. Thermal ellipsoid plot of the cluster anion **2** of [PPN][Fe$_3$-Mn(CO)$_{12}(\mu_4$-O)] (40% probability).

the orientation of the hinge carbonyl ligands is quite different in the two clusters. The structure and bonding of the butterfly cluster HFe$_4$(CO)$_{12}$CH have been viewed by Fehlner and Housecroft[38] as the addition of an Fe(CO)$_3$ fragment to a triiron−CH core; the disposition of carbonyl ligands in the butterfly product is arrived at by rotation of the two hinge Fe-(CO)$_3$ groups relative to their orientations in the triangular cluster. This rotation opens the side of the metal triangle for bonding to the fourth Fe(CO)$_3$ group and orients the hinge Fe-(CO)$_3$ fragment orbitals properly to bond effectively to both wingtip metal atoms of the butterfly. The orientation of the hinge-bound carbonyl ligands in **2** is a consequence of this rotation not being complete. Additionally, two apparent semibridging interactions exist between two of the carbonyl ligands bound to the hinge iron atoms and manganese (Mn1−C2 = 2.675(5) Å, Mn1−C5 = 2.736(5) Å).

The oxo ligand in **2** is bound at a slightly shorter distance to the wingtip metal atoms than the hinge metal atoms. These M−O distances are similar to the Fe−O distances observed in the structure of **1**. In the carbide and nitride clusters, **7** and **8**, respectively, the M$_w$−E distances are considerably shorter than the M$_h$−E distances (see Table 9). The M−O distances in **2** are most similar to the longer M$_h$−E distances in **7** and **8**. These trends are not in agreement with expectations based on the difference in size in progressing from carbon to oxygen but must be related to differences in the bonding in **2** (see discussion below).

(36) Boehme, R. F.; Coppens, P. *Acta Crystallogr., Sect. B: Struct. Sci.* **1981**, *B37*, 1914.
(37) Fjare, D. E.; Gladfelter, W. L. *Inorg. Chem.* **1981**, *20*, 3533.
(38) Fehlner, T. P.; Housecroft, C. E. *Organometallics* **1984**, *3*, 764.

Variable-Temperature ^{13}C NMR Spectra of Butterfly Oxo Clusters.

^{13}C NMR spectroscopy was utilized for characterization of the mixed-metal oxo clusters. The samples for ^{13}C NMR analysis were synthesized by using [Fe$_3$(*CO)$_9$(μ_3-O)]$^{2-}$ that is enriched to ~35% ^{13}C at the carbonyl ligands. Complete ^{13}CO scrambling was observed in all reactions and resulted in enrichment of the carbonyl ligands bound to the heterometal, in addition to the iron atoms in the butterfly products.

The variable-temperature ^{13}C NMR spectra for **2** are pictured in Figure 2, and the data for selected temperatures are summarized in Table 10. At 20 °C in CD$_2$Cl$_2$/CHFCl$_2$ solution (1: 2), only two resonances are observed in the ^{13}C NMR spectrum of **2**. The deshielded resonance (intensity 3) is assigned to the manganese-bound carbonyl ligands while the remaining peak (intensity 9) is assigned to the iron-bound carbonyl ligands. Exchange does not occur between the CO ligands bound to the two types of metal atoms on this time scale. Between +20 and −50 °C, the peak due to iron-bound carbonyl ligands collapses to the baseline and then reappears as two resonances of ratio 3:6. This pattern is consistent with the number of inequivalent metal sites present in the solid-state structure of C_{2v} symmetry, thus implying that CO is localized on individual metal centers.

Localized turnstile exchange, which equilibrates the three carbonyl ligands of each M(CO)$_3$ fragment, is usually the lowest energy fluxional process in metal−carbonyl clusters.[39,40] This exchange is frozen out for the wingtip manganese atom at −110 °C and for the wingtip iron at −130 °C. At the lowest temperature achieved, the peaks due to the three distinct resonances expected for the hinge-bound carbonyl ligands have not yet sharpened.

The simplest mechanism for equilibration of the iron-bound carbonyl ligands at room temperature is triiron-triangle localized exchange. Intermetallic CO scrambling has been shown to readily occur in heterometallic clusters, such as Co$_2$Fe(CO)$_9$-(μ_3-S).[41] The disposition of the carbonyl ligands in the triiron portion of **2** is similar to that of the parent cluster **1**, so it seems likely that the delocalized exchange process would be favorable. Alternatively, an exchange process which involves manganese−iron bond cleavage, with fluctional bonding of the Mn(CO)$_3$ unit to each edge of the Fe$_3$O triangle could explain this variable-temperature behavior. This process involves formation of an unsaturated intermediate and would be expected to occur more readily in a coordinating solvent. The coalescence temperature in acetone-d_6 solution is nearly identical to that in CD$_2$Cl$_2$ solution, disfavoring the latter mechanism.

The ^{13}C NMR spectra indicate that **3** is isostructural with **2**. A 9:3 pattern is observed in the ^{13}C NMR spectrum of **3** at room temperature (see Table 10). The resonance for the Re-bound carbonyl ligands occurs at 193.9 ppm and is shielded with respect to the resonance for the Fe-bound carbonyl ligands at 211.2 ppm. At −70 °C, distinct resonances for the hinge and wingtip iron atom carbonyl ligands are observed as well as the expected 2:1 pattern for the Re-bound CO ligands.

Coordination Chemistry of Sulfido Ligands in Metal−Carbonyl Clusters.

In contrast to the paucity of oxo carbonyl clusters, many higher nuclearity sulfido carbonyl clusters are known. Common coordination environments for cluster-bound sulfido ligands, **VI−VIII**, are shown below.[42] Coordination of

VI   VII   VIII

Table 9. Structural Parameters of μ_4-E Butterfly Clusters[a]

cluster	[Fe₃Mn(CO)₁₂O]⁻	[Fe₄(CO)₁₂C]²⁻	[Fe₄(CO)₁₂N]⁻	[Fe₃Mn(CO)₁₂S]⁻	[Fe₄(CO)₁₂CCO₂Me]⁻
no.	2	7	8	5	9
M_h–E, Å	1.902(4)	1.96(3)	1.900(6)	2.222(1)	1.955(4)
M_w–E, Å	1.872(3), 1.877(3)[b]	1.80(3)	1.771(5)	2.275(1)	2.02(1)
M_w–M_h, Å	2.517(2), 2.61(2)[b]	2.64(1)	2.604(7)	2.589(2)	2.500(9)
M_h–M_h, Å	2.499(1)	2.533(2)	2.512(1)	2.561(1)	2.587(1)
M_w–E–M_w, deg	168.3(1)	176.3(4)	179.0(3)	131.31(5)	148
M_w–M_h–M_h–M_w, deg	113	102	102	134	130
ref	this work	36	37	this work	44

[a] Key: M_w, wingtip metal atom; M_h, hinge metal atom. [b] For the first entry, M = Fe; for the second entry, M = Mn.
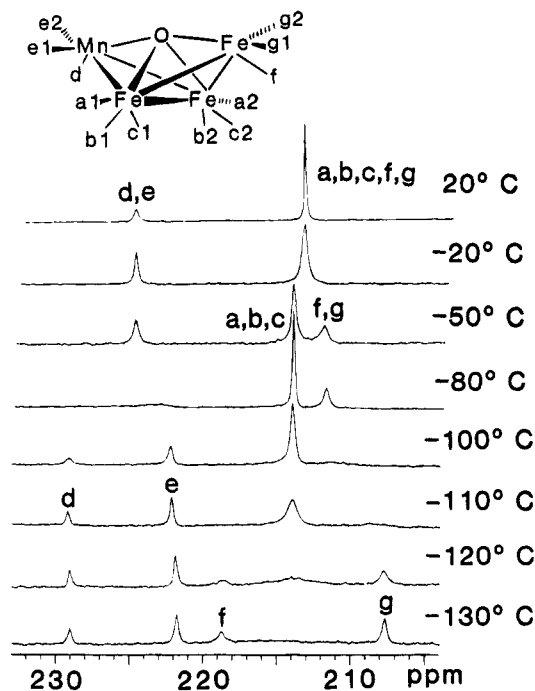
Figure 2. Variable-temperature ¹³C NMR spectra for the carbonyl ligands of [Fe₃Mn(CO)₁₂(μ_4-O)]⁻, **2**.

a sulfido ligand in a butterfly arrangement of metal atoms has not been demonstrated for a system which contains carbon monoxide as the only other ligand. In fact, there is an example in which a μ_3-S tetrahedral cluster is favored over a μ_4-S butterfly.[43] Thermal decarbonylation of the tetraosmium butterfly cluster Os₄(CO)₁₃(μ_3-S) yields the tetrahedral cluster Os₄(CO)₁₂(μ_3-S); both the starting material and the product contain μ_3-sulfido ligands (see Scheme 1). Since the *closo* tetrahedral product has one more Os—Os bond than the hypothetical Os₄S butterfly, the course of this reaction may be governed by the strength of Os—Os bonds. The four-metal sulfido systems described below are based on a Fe₃ core and contain primarily first-row transition metals; weaker Fe—M bonds may favor formation of a μ_4-S butterfly cluster.

Synthesis of Four-Metal Sulfido Clusters. The synthetic methods are similar to those employed for the synthesis of four-metal oxo clusters above, except [Fe₃(CO)₉(μ_3-S)]²⁻ (**4**) is used as the starting cluster. Reactions between **4** and [Mn(CO)₃(NCCH₃)₃]⁺ proceed smoothly in acetone solution to generate

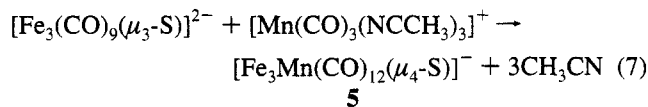(39) Aime, S.; Milone, L. *Prog. NMR Spectrosc.* **1977**, *11*, 183.
(40) Band, E.; Muetterties, E. L. *Chem. Rev.* **1978**, *78*, 639.
(41) Aime, S.; Milone, L.; Rossetti, R.; Stanghellini, P. L. *Inorg. Chim. Acta* **1977**, *25*, 103.
(42) Adams, R. D. *Polyhedron* **1985**, *4*, 2003.
(43) Adams, R. D.; Horvàth, I. T.; Segmüller, B. E.; Yang, L.-W. *Organometallics* **1983**, *2*, 1301.

Table 10. Variable-Temperature ¹³C NMR Data for the CO Ligands in Heterometallic Butterfly Oxo and Sulfido Clusters[a,b]

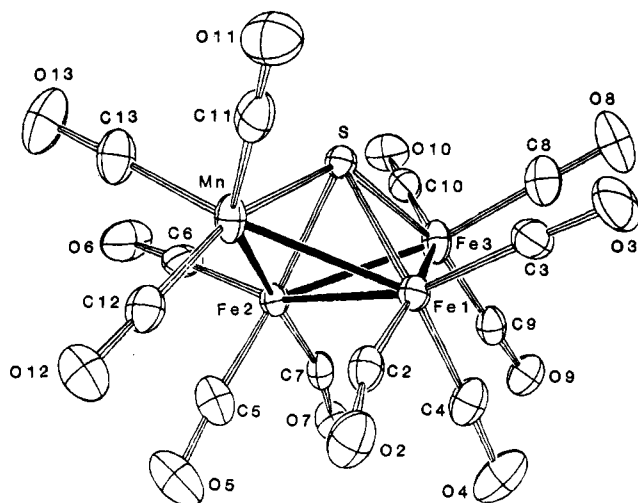| compd	temp, °C	¹³C NMR data, ppm
[PPN][Fe₃Mn(CO)₁₂(μ_4-O)][c] ([PPN]**2**)	20	226.0(3), 214.5(9)
	−50	225.6(3), 214.8(6), 212.7(3)
	−110[d]	229.7(1), 222.6(2)
	−130[e]	219.3(1), 208.2(2)
[PPN][Fe₃Re(CO)₁₂(μ_4-O)][f] ([PPN]**3**)	10	211.2(9), 193.9(3)
	−70	210.9(6), 210.0(3), 199.6(1), 190.1(2)
[PPN][Fe₃Mn(CO)₁₂(μ_4-S)][c] ([PPN]**5**)	20	224.7(3), 217.1(9)
	−30	224.2(3), 218.5(6), 213.0(3)
	−90	226.2(1), 222.0(2), 218.1(6), 212.4(3)
[PPN][Fe₃Re(CO)₁₂(μ_4-S)][f] ([PPN]**6**)	−20	214.9(6), 211.2(3), 193.8(4)
	−90	214.3(6), 210.5(3), 196.5(1), 191.5(2)

[a] The solvent resonance (CD₂Cl₂, δ = 53.8) was used as an internal reference. [b] The numbers in parentheses are the relative integrated intensities. [c] Spectra recorded in CD₂Cl₂/CHFCl₂ (ca. 1:2). [d] Only the resonances for the wingtip manganese atom are reported. [e] Only the resonances for the wingtip iron atom are reported. [f] Spectra recorded in CD₂Cl₂.

Scheme 1
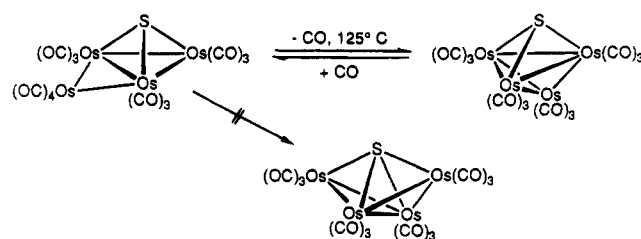
the Fe₃MnS cluster (eq 7). Re(CO)₅(OSO₂CF₃) was again found

$$[Fe_3(CO)_9(\mu_3\text{-}S)]^{2-} + [Mn(CO)_3(NCCH_3)_3]^+ \longrightarrow$$
$$[Fe_3Mn(CO)_{12}(\mu_4\text{-}S)]^- + 3CH_3CN \quad (7)$$
$$\mathbf{5}$$

to be the best reagent to synthesize the mixed-metal Fe₃Re—sulfido cluster. Reactions between **4** and Re(CO)₅(OSO₂CF₃) generate a stable intermediate cluster with a pendant Re(CO)₅ cap (eq 8). This intermediate cluster loses two molecules of

$$[Fe_3(CO)_9(\mu_3\text{-}S)]^{2-} + Re(CO)_5(OSO_2CF_3) \longrightarrow$$
$$[Fe_3(CO)_9(\mu_3\text{-}SRe(CO)_5)]^- + [SO_3CF_3]^- \quad (8)$$
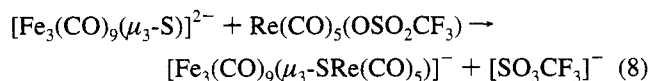
carbon monoxide in refluxing 1,2-dichloroethane to generate

Figure 3. Thermal ellipsoid plot of the cluster anion **5** of [PPN][Fe$_3$-Mn(CO)$_{12}$(μ_4-S)] (40% probability).

the corresponding Fe$_3$ReS cluster (eq 9). The details involved

$$[Fe_3(CO)_9(\mu_3\text{-}SRe(CO)_5)]^- \xrightarrow{\Delta}$$

$$[Fe_3Re(CO)_{12}(\mu_4\text{-}S)]^- + 2CO \quad (9)$$
$$\mathbf{6}$$
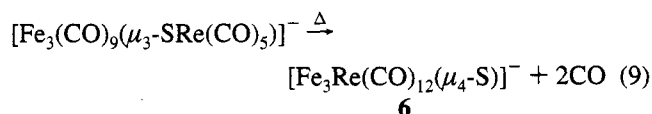
in this conversion will be discussed elsewhere.[9b] The patterns observed in the infrared spectra (see Table 8) as well as the ^{13}C NMR spectra (see below) for the four-metal sulfido products are very similar to those observed for the butterfly oxo clusters, favoring formulation of the products as μ_4-S butterfly clusters.

Structure of [PPN][Fe$_3$Mn(CO)$_{12}$(μ_4-S)] ([PPN]5). The structure of the cluster anion **5**, as determined by single-crystal
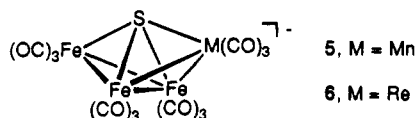
X-ray diffraction, is depicted in Figure 3. The four-metal sulfido clusters do contain a μ_4-sulfido ligand. The cluster has an approximate noncrystallographic 2-fold axis that passes through the sulfur atom and the centroid of the Fe1−Fe2 bond. Although one of the wingtip metal atoms is labeled Mn, it is clear from the observed metric parameters that the manganese atom must be disordered between the wingtip positions. This feature probably accounts for the elongation of the thermal ellipsoids of the wingtip metal atoms.

The appearance of the butterfly sulfido cluster is strikingly different from that of the corresponding oxo cluster. Due to the larger size of sulfur, the dihedral angle between the two wings of the butterfly has opened to 134°, which is approximately 20° greater than in the oxo cluster. The Mn−S−Fe3 angle (131°) is considerably more acute than that for the oxo cluster, **2** (168°), the carbido cluster, **7** (179°),[36] or the nitrido cluster, **8** (176°). The geometry of **5** may be best described as a trigonal bipyramid, where sulfur is one of the vertices of the polyhedron. In these respects, the structure of **5** is very similar to the cluster [Fe$_4$(CO)$_{12}$(μ_4-CCO$_2$Me)]$^-$ (**9**),[44] where the butterfly dihedral angle is 130° and the angle at the μ_4-C is 148°. The structure of **5** also resembles that of **9** in the metal−E bonding. The M$_w$−E distances in these two clusters

are slightly longer than the M$_h$−E distances. The μ_4-S butterfly geometry has been observed for other clusters that contain several sulfido ligands.[8] The structure of **5** is very similar to those of these other butterfly clusters.

Variable-Temperature ^{13}C NMR Spectra of Butterfly Sulfido Clusters. Samples for analysis by ^{13}C NMR spectroscopy were prepared from reactions with [Fe(*CO)$_9$(μ_3-S)]$^{2-}$ enriched to ~30% [13]C at the carbonyl ligands. As for **2** and **3**, complete *CO scrambling was observed resulting in enrichment of all carbonyl ligands in the butterfly products. The ^{13}C NMR data for **5** and **6** are summarized in Table 10. The variable-temperature behavior is very similar to that of **2**, confirming that **5** and **6** are isostructural with the butterfly oxo clusters. For **5**, at room temperature, the peak corresponding to the iron-bound carbonyl ligands starts to broaden, and at −30 °C, two distinct resonances are observed for the hinge and wingtip Fe-bound carbonyl ligands. At −90 °C, turnstile rotation is frozen out on the wingtip Mn(CO)$_3$ group, and a 2:1 pattern is observed for the Mn-bound CO ligands. The room-temperature resonances for the Fe-bound CO ligands in **6** are even broader at room temperature, and at −20 °C, distinct resonances are observed for the hinge and wingtip Fe-bound carbonyl ligands.

The ^{13}C NMR resonances for the parent oxo and sulfido clusters, **1** and **4**, are nearly identical (see Table 6). Upon coordination of an additional metal atom to form the butterfly cluster, differences are observed in the resonances for the Fe-bound carbonyl ligands of the oxo and sulfido clusters. For both **2** and **3**, the average resonance for the Fe-bound carbonyl ligands is deshielded with respect to the average resonance for **5** and **6**. This would be consistent with more electron density on the sulfido clusters than on the oxo clusters. Substitution of Re(CO)$_3$ for Mn(CO)$_3$ results in more shielded resonances for the Fe-bound carbonyl ligands in both the oxo and sulfido butterflies, suggesting that Re withdraws more electron density from the Fe$_3$(CO)$_9$E cluster than Mn.

Bonding in the Butterfly Oxo and Sulfido Clusters. The butterfly framework of metal atoms is less able to accommodate ligands of different sizes than the [Fe$_3$(CO)$_9$(μ_3-E)]$^{2-}$ clusters described above. This inflexibility affects both the geometry and bonding of the butterfly clusters. Earlier calculations showed that the molecular orbitals of the cluster can be divided into groups that are localized on the metal framework and groups that represent metal−ligand interaction.[45] In order to maintain the stability of the cluster, changes in the cluster which lead to the weakening of one set of interactions generally strengthen the other set of interactions. Apparently a delicate balance between metal−metal and metal−ligand interactions determines the observed geometries in butterfly oxo and sulfido clusters. A recent paper compared the bonding of the complexes [Fe$_4$-(CO)$_{12}$(μ_4-C)]$^{2-}$ and [Fe$_4$(CO)$_{12}$(μ_4-N)]$^-$ with a model oxo compound [Fe$_4$(CO)$_{12}$(μ_4-O)],[46] and these relatively small changes in heteroatom sizes had significant consequences.

Bonding in [Fe$_3$Mn(CO)$_{12}$(μ_4-O)]$^-$ (2). The structural features of the mixed-metal oxo cluster, **2**, are not very similar to those of the more symmetric homometallic carbide and nitride clusters, **7** and **8**, respectively (see above), suggesting that the bonding in **2** is different. The character of the metal bonding orbitals in **2** is illustrated in Figure 4c. Orbitals are illustrated in Figure 4a,b for [Fe$_3$Mn(CO)$_{13}$(μ_4-C)]$^-$, in which the manganese atom occupies a hinge position,[47] and the carbide cluster, **7**,[45] respectively. As expected, the orbitals for **2** are consider-

(44) Bradley, J. S.; Harris, S.; Newsan, J. M.; Hill, E. W.; Leta, S.; Modrick, M. A. *Organometallics* **1987**, *6*, 2060.

(45) Harris, S.; Bradley, J. S. *Organometallics* **1984**, *3*, 1086.
(46) Harris, S.; Blohm, M. L.; Gladfelter, W. *Inorg. Chem.* **1989**, *28*, 2290.
(47) Hriljac, J. A.; Harris, S.; Shriver, D. F. *Inorg. Chem.* **1988**, *27*, 816.
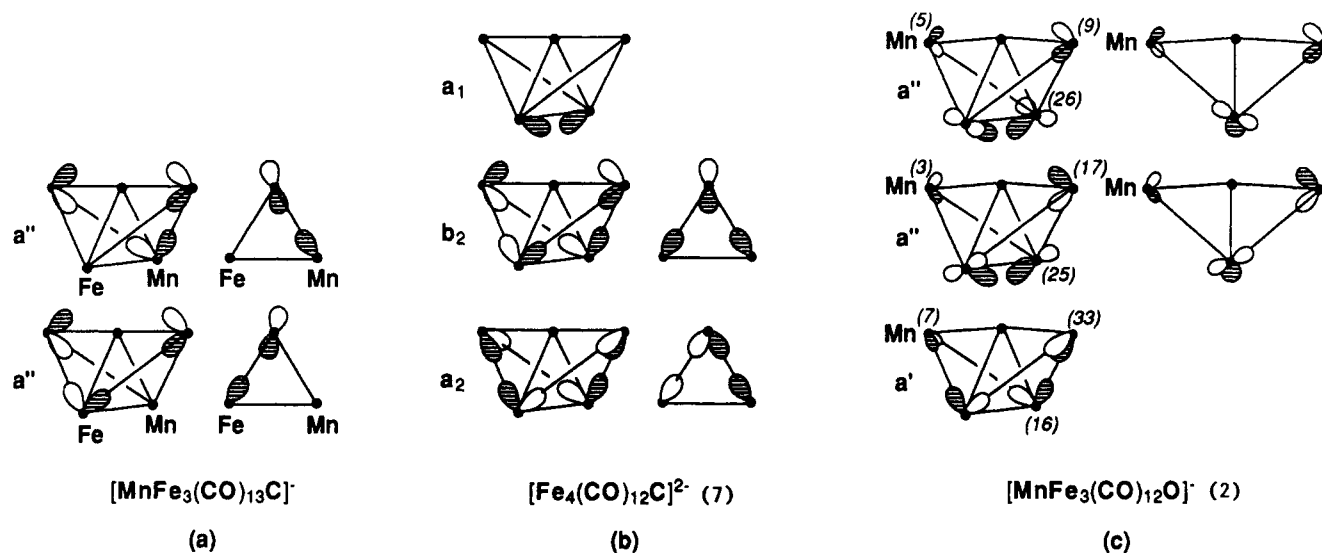
Figure 4. Character of the metal bonding orbitals in (a) [Fe₃Mn(CO)₁₃C]⁻, (b) [Fe₄(CO)₁₂C]²⁻ (7), and (c) [Fe₃Mn(CO)₁₂O]⁻ (2). The metal orbital percent character is indicated for each of the molecular orbitals in (c).

Table 11. M—M Overlap Populations

	Feₕ—Feₕ	Feₕ—Feᵥᵥ	Feₕ—Mn
[Fe₄(CO)₁₂(μ₄-C)]²⁻ [a]	0.075	0.036	
[Fe₃Mn(CO)₁₂(μ₄-O)]⁻	0.060	0.050	0.015
[Fe₃Mn(CO)₁₂(μ₄-S)]⁻	0.066	0.056	0.040

[a] Reference 44.

ably different from those shown for either **7** or [Fe₃Mn(CO)₁₃-(μ₄-C)]⁻. It is convenient to relate the new orbitals in the lower symmetry clusters to the orbitals in **7**. In [Fe₃Mn(CO)₁₃(μ₄-C)]⁻, the two a″ orbitals (Figure 4a) can be viewed as combinations of the 3a₂ and 5b₂ orbitals of **7** (Figure 4b). These two a″ orbitals allow the hinge atoms to interact separately with the two wingtip atoms. In **2**, the two a″ orbitals (Figure 4c) can be viewed as combinations of the 5b₂ and 6a₁ orbitals of **7**. These combinations result in more localized bonding within the Fe₃ triangle.

The percent character of each metal atom in the three metal-based orbitals is also included in Figure 4c. These values indicate that the interactions between the Mn(CO)₃ group and the triangular metal framework are relatively weak compared to those among the Fe atoms in the metal triangle. This trend is also reflected in the metal—metal overlap populations listed in Table 11. The Feₕ—Feₕ overlap in **2** is only slightly greater than the Feₕ—Feᵥᵥ overlap, unlike for **7**, where these values differ by a factor of 2. The small Feₕ—Mn overlap population indicates that the Feₕ—Mn bond is considerably weaker than the Fe—Fe bonds.

The geometry of the cluster is such that two of the hinge carbonyl ligands might be viewed as semibridging to the Mn atom (see above). Such an interaction would at least partly compensate for the weak direct Fe—Mn bond. Metal—carbon overlap populations indicate that this is not the case, however, since the overlap population between the carbon atoms of the "semibridging" carbonyl ligands and the Mn atom is negligible. The slight bending back of these two carbonyl ligands probably comes about because of steric crowding.

The M—O overlap populations for **2** are shown in Table 12. The strengths of the M—O bonding interactions in **2** are more regular than those of the M—C interactions in **7**. In **7**, where the two wingtip Fe atoms and the μ₄-C atom are nearly collinear, a combination of σ and π interactions between the C and wingtip Fe atoms leads to strong Feᵥᵥ—C bonding. In **2**, where the

Mᵥᵥ—O distances are longer and the O atom is not collinear with the two wingtip metal atoms, the π interactions are nearly lost. Although the Mn—Feₕ bonds are considerably weaker than the Fe—Fe bonds, the Mn—O and Feₕ—O overlap populations are comparable.

The bonding picture which emerges from these comparisons is one in which the Mn atom interacts primarily with the O atom and only weakly with the two Fe atoms of the Fe₂Mn triangle. The triiron unit reorganizes only slightly to interact with the Mn atom. To understand why the observed geometry is preferred over the more symmetric butterfly, it is useful to compare the bonding in the more symmetric [Fe₄(CO)₁₂(μ₄-C)]²⁻, [Fe₄(CO)₁₂(μ₄-N)]⁻, and model cluster, Fe₄(CO)₁₂(μ₄-O).⁴⁶ In these clusters, when the μ₄-ligand is colinear with the two wingtip metal atoms, the stability of the cluster geometry decreases as the size of the μ₄-ligand decreases. This feature is a result of the much weaker π interactions between the smaller ligand pₓ and p₂ orbitals and the wingtip metal atoms. While an adjustment to the cluster framework that opens up the dihedral angle and shortens the metal—metal bonds leads to stronger metal—metal bonding, this deformation further weakens the metal—L interaction. Clearly, a delicate balance between the optimization of the metal—metal and metal—oxygen bonds will govern the configuration of oxo butterfly clusters. The observed configuration in **2** allows relatively strong Fe—Fe bonding to be maintained within the Fe₃O unit while a substantial Mn—O interaction develops. This occurs, however, at the expense of the Mn—Fe bonds. The observed asymmetric structure suggests that any strengthening of the Mn—Fe bonds in a more symmetric structure would not be sufficient to compensate for the necessary weakening of the Feₕ—Feᵥᵥ bonds. The more open geometry of the oxo cluster appears to be a consequence of the small size of the O atom, a nonintiutive result.

Bonding in [Fe₃Mn(CO)₁₂(μ₄-S)]⁻ (5). The structure of **5** suggests that the bonding in this cluster is much more symmetric than the bonding in **2**, which is reflected in the character of the metal—metal bonding orbitals. The three metal—metal bonding orbitals in **5** are similar to the orbitals shown in Figure 4b for the carbide cluster, **7**. Like the 6a₁ orbital in **7**, the HOMO in **5** is localized across the hinge. The other two orbitals resemble the 5b₂ and 3a₂ orbitals in **7**, except that now the Mn character is only about half as large as the Feᵥᵥ character in these two orbitals. Thus the metal—metal bonding is less localized around

Table 12. E−M Overlap Populations in Butterfly Clusters

	$[Fe_4(CO)_{12}(\mu_4\text{-}C)]^{2-}$ [a]		$[Fe_3Mn(CO)_{12}(\mu_4\text{-}O)]^-$			$[Fe_3Mn(CO)_{12}(\mu_4\text{-}S)]^-$		
	Fe_h	Fe_w	Fe_h	Fe_w	Mn	Fe_h	Fe_w	Mn_w
$E(p_x)$−$M(d,s,p)$	0.084	0.040	0.094	0.001	0.008	0.087	−0.001	0.003
$E(p_y)$−$M(d,s,p)$	0.000	0.162	−0.005	0.144	0.141	−0.001	0.131	0.112
$E(p_z)$−$M(d,s,p)$	0.081	0.047	0.076	0.002	0.011	0.082	0.001	0.002
total	0.165	0.249	0.165	0.147	0.160	0.168	0.131	0.117

[a] Reference 45.

the triiron unit in the sulfido cluster than in the oxo cluster, but the Fe−Fe bonds are still stronger than the Fe−Mn bonds. The metal−metal overlap populations listed in Table 11 are consistent with this picture. These overlap populations also indicate that all of the metal−metal bonds in the sulfido cluster are stronger than the corresponding bonds in the oxo cluster. The higher Fe−Fe overlap populations in the sulfido cluster **5** are remarkable because the sulfido clusters have longer Fe−Fe bonds than their oxo counterparts.

The positions of the hinge carbonyl ligands in **5** indicate that some of these ligands might be viewed as semibridging to the hinge metal atoms. Just as in the oxo cluster, however, the metal−carbon overlap populations indicate that there is no bonding interaction between these hinge carbonyl ligand and the wingtip metal atoms. Once again, the observed geometry is probably the result of steric crowding.

The M−S overlap populations, listed in Table 12, indicate that the Mn−S and Fe_w−S bonding interactions are considerably weaker than the Fe_h−S bonding interactions. This is consistent with the trends observed in other butterfly clusters having very open frameworks. (In $[Fe_4(CO)_{12}CC(O)CH_3]^-$, for example, the Fe_h−C and Fe_w−C overlap populations are 0.175 and 0.139, respectively.[45])

The picture of the bonding in **5** that emerges from these comparisons is quite straightforward. The S atom is so large that the butterfly framework must flatten in order for all four metal atoms to bond with the S atom. The S atom sits well outside the metal framework, and the actual cluster geometry represents a compromise between the optimization of metal−sulfur and metal−metal bonding. The observed geometry leads to the formation of relatively strong metal−metal bonding at the expense of metal−sulfur bonding. Thus the large S atom affects the cluster bonding and structure in a more intuitive way than the smaller O atom.

Because of the apparent disorder of the Mn atoms among the wingtips, the reported structure of **5** may be more symmetric than that of the actual cluster. This means that the calculated molecular orbitals may also be more symmetric than those in the actual cluster. For this reason, calculations were also carried out for a less symmetric cluster geometry in which the 2-fold axis was replaced by a mirror plane (as in **2**). The results of the calculations for this cluster showed that although the Mn contribution to the metal−metal bonding orbitals decreased by a few percent, the much more localized orbitals seen in the oxo cluster did not occur. Thus, the calculations may slightly overemphasize the differences between the bonding in the oxo and sulfido clusters, but these differences are real and can be related to the relative sizes of the O and S atoms.

Summary and Conclusions. Addition of $[M(CO)_3]^+$ (M = Mn, Re) fragments to the trinuclear clusters $[Fe_3(CO)_9(\mu_3\text{-}E)]^{2-}$ (E = O, S) results in the formation of μ_4-E butterfly clusters in which the heteroatom occupies a wingtip position in the butterfly arrangement of metal atoms. Butterfly clusters are formed preferentially over the possible electron-precise tetrahedral clusters with a face-capping μ_3-E ligand. The structures and
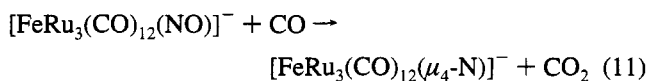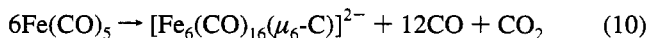
bonding of the oxo and sulfido clusters are quite different. The open butterfly geometry of the oxo cluster results from the small size of the oxygen atom and the weak π-bonding interactions between the oxygen atom and the wingtip metal atoms. The observed cluster geometry indicates strong Fe−Fe bonding within the Fe_3 triangle at the expense of Fe−Mn bonding. The large dihedral angle in the sulfur cluster is a consequence of the large size of the sulfur atom. The metal−metal bonding is more symmetric in the sulfido cluster than in the oxo cluster, but the π bonding between the sulfur atom and wingtip metal atoms is also weak in this cluster.

The rarity of the μ_4-E configuration for previously reported metal carbonyl clusters with heavy main group atoms as ligands may be a consequence of the cluster-building reagents generally employed. A favorable bonding mode in which the metal carbonyl group is appended to the sulfur (see **IX**) is observed

IX
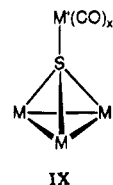
for $[Fe_3(CO)_9(\mu_3\text{-}SRe(CO)_5)]^-$ and several sulfido clusters, $[H_{2-n}Fe_3(CO)_9(\mu_3\text{-}S)]^{n-}$ (n = 0−2), with pendant $M(CO)_5$ fragments (M = Cr, W).[48] Thermolysis of the intermediate cluster, $[Fe_3(CO)_9(\mu_3\text{-}SRe(CO)_5]^-$, with expulsion of 2 equiv of CO, is required to produce the butterfly cluster. The open butterfly framework, necessitated by the large size of the sulfur atom, results in interactions between the wingtip metal atoms and the sulfur that are considerably weaker than those observed for first-row main group atoms such as C and N. Under reaction conditions where CO is present, or with reagents that have extra carbonyl ligands bound to the metal atom, a geometry which allows strong M′−S bonding and strong M−M bonding within the M_3 triangle as in **IX** is favored. In fact, both the butterfly sulfido clusters **5** and **6** react with CO to coordinate additional carbonyl ligands to the heterometal.[9b]

The rarity of low-valent oxo clusters seems surprising, given the vast chemistry which has been developed for carbonyl clusters containing substituent-free carbon and nitrogen ligands. A tendency to decompose with the loss of CO_2 from carbonyl-containing compounds may, in part, offer an explanation. Carbido[49] and nitrido[50] clusters are commonly synthesized from cleavage of coordinated CO and NO ligands (eqs 10 and 11).

$$6Fe(CO)_5 \rightarrow [Fe_6(CO)_{16}(\mu_6\text{-}C)]^{2-} + 12CO + CO_2 \qquad (10)$$

$$[FeRu_3(CO)_{12}(NO)]^- + CO \rightarrow$$
$$[FeRu_3(CO)_{12}(\mu_4\text{-}N)]^- + CO_2 \quad (11)$$

The intermediates proposed to facilitate these cleavage reactions involve simultaneous coordination of both carbon and oxygen (or nitrogen and oxygen) to the metal framework. These reactions could potentially yield products that also contain
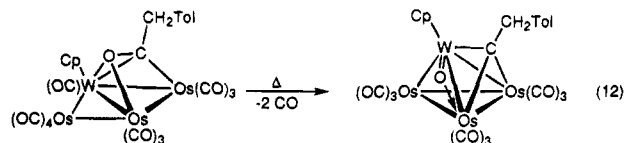
an oxo ligand, but under the reaction conditions, the oxo ligand is lost as CO_2. Cleavage of the carbon–oxygen bond in the acyl cluster $CpWOs_3(CO)_{11}(\mu_3\text{-}\eta^2\text{-}C(O)CH_2Tol$ $(Cp = \eta^5\text{-}C_5H_5,$ $Tol = p\text{-}C_6H_4CH_3)$ yields a product that contains an oxo ligand bridging W and Os (eq 12),[51] illustrating that in the presence of a more oxophilic metal, the oxo ligand can be maintained in the coordination sphere of a cluster. However, for later transition metal systems, oxygen atom transfer to carbon monoxide appears to be an important process.

$$(12)$$

Supporting Information Available: Complete tables of crystallographic data, positional parameters, anisotropic thermal parameters, and bond lengths and angles for **5** and a figure showing the numbering scheme for $[(PPh_3)_2N]^+$ (19 pages). Ordering information is given on any current masthead page.

IC941251+

(48) Takács, J.; Markó, L. *Transition Met. Chem.* **1985**, *10*, 21.
(49) Churchill, M. R.; Wormald, J.; Knight, J.; Mays, M. J. *J. Am. Chem. Soc.* **1971**, *93*, 3073.
(50) Fjare, D. E.; Gladfelter, W. L. *J. Am. Chem. Soc.* **1984**, *106*, 4799.
(51) Shapley, J. R.; Park, J. T.; Churchill, M. R.; Ziller, J. W.; Beanan, L. R. *J. Am. Chem. Soc.* **1984**, *106*, 1144.